Biomaterials Journal
http://www.biomatj.com
Online ISSN: 2812-5045

Type of the Paper (Research Article)

Preparation, characterization, and functional properties of ternary composite nanoparticles for enhanced bioaccessibility and antitumor activity of cannabidiol

Zhoushan Wu[a,b], Guiguang Cheng[c,], Yaping Liu[c], Jiawei Zhao[a,b], Ganpeng Li[a], Minglong Yuan[b,*]and Yudan Wang [a,b,*]

Citation: *Zhoushan Wu, Guiguang Cheng, Yaping Liu, Jiawei Zhao, Ganpeng L[a], Minglong Yuanand Yudan Wang. Preparation, characterization, and functional properties of ternary composite nanoparticles for enhanced bioaccessibility and antitumor activity of cannabidiol . Biomat. J., 4 (1), 8 – 36 (2025).*

https://doi.org/10.5281/znodo.5829408

Received: 8 May 2024
Accepted: 21 December 2024
Published: 25 January 2025

[a] Key Laboratory of Chemistry in Ethnic Medicinal Resources, State Ethnic Affairs Commission and Ministry of Education, Yunnan Minzu University, Kunming 650500, China

[b]School of Chemistry and Environment, National and Local Joint Engineering Research Center for Green Preparation Technology of Biobased Materials, Yunnan Minzu University, Kunming 650500, China

[C] The faculty of Food Science and Engineering, Kunming University of Science and Technology,Kunming 650500, China

* Corresponding author e-mail: yml@ynni.edu.cn (M. Yuan), wangyudan@ymu.edu.cn (Y. Wang).
These authors have contributed equally to this work.

Abstract: Cannabidiol (CBD) faces challenges in food and pharmaceutical use due to poor solubility and stability. A novel CBD delivery system using stearic acid-modified Bletilla striata polysaccharides (SA-BSPs) was developed, improving encapsulation and release. Optimal encapsulation efficiency (92.07%) and loading capacity (8.94%) were achieved with a 3:10 CBD to SA-BSPs ratio. The system showed sustained release over a week and strong binding affinity to CB1 receptors. CBD-SA-BSPs copolymer micelles effectively suppressed the proliferation and reduced the viability of MHCC-97H and HCCLM3 cells, particularly the CBD-SA-BSPs (3:10) at a concentration of 20 μg/mL. Compared with the model group, the levels of IL-2, IL-6, and TNF-α in the serum of mice in the drug-administered groups were significantly reduced, suggesting that the drug may exert its anti-hepatocarcinoma effect by regulating the levels of these cytokines. In vivo study results showed that the tumor inhibition rate of 10mg/kg CBD-SA-BSPs (3:10) group was as high as 72.83%, revealing polymer micelles have potential for future therapeutic applications.

Keywords: *Cannabidiol; Stearic acid-modified Bletilla striata polysaccharides; Self-assembled micelles; Drug delivery; Antitumor activity; Liver cancer*

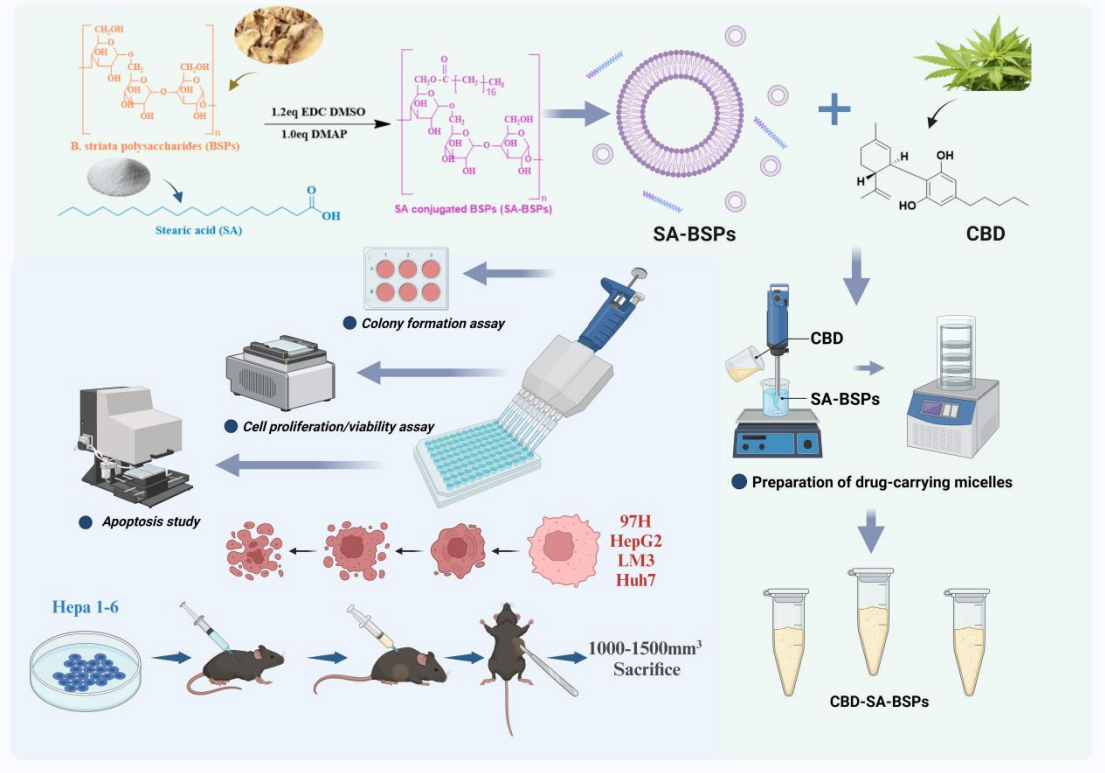

Scheme 1. Schematic representation of the synthesis of SA-BSPs and CBD-SA-BSPs.

1. Introduction

Liver cancer presents a substantial global health challenge, particularly in Asia, where recent years have seen high incidence and mortality rates [1]. Chronic hepatitis B virus (HBV) and hepatitis C virus (HCV) infections, along with alcohol abuse, are closely linked to liver damage and carcinogenesis [2]. Current treatment methodologies include surgical resection, radiation therapy, targeted drugs, and chemotherapy, but improved strategies are needed, especially for advanced-stage patients [3].In recent years, substantial attention has been devoted to exploring the potential of cannabidiol (CBD), a natural compound, due to its multifaceted physiological properties, which encompass anti-inflammatory, antioxidant, and antitumor effects. CBD, derived from cannabis, is a non-psychoactive cannabinoid with a diverse range of therapeutic characteristics, including anti-seizure, anti-anxiety, antipsychotic, and antitumor activities, while maintaining a commendable safety and tolerability profile [4]. Increasing research suggests the promise of CBD in liver cancer treatment, working through various mechanisms, including promoting cellular apoptosis, inhibiting cell proliferation, and modulating the tumor microenvironment, thereby suppressing the growth and spread of liver cancer [5]. Nevertheless, despite preliminary studies indicating the potential value of CBD in liver cancer therapy, further clinical research is needed to fully comprehend its efficacy and safety [6]. However, the

utilization of CBD as a pharmaceutical agent is hindered by its intrinsic characteristics, including low bioavailability, poor water solubility, and variable pharmacokinetics.

CBD is highly sensitive to environmental factors, including heat, light, and oxygen, which can lead to isomerization, polymerization, or degradation. These factors limit its widespread use in the food and pharmaceutical industries [7]. Additionally, CBD faces challenges in oral absorption due to its poor solubility in the gastrointestinal tract, resulting in a low bioavailability of only 6%. Therefore, it is crucial to develop a delivery system that can encapsulate and protect CBD while improving its bioavailability. In recent years, various delivery systems have been developed for CBD encapsulation, such as nanoemulsions [8,9], Pickering emulsions [10], and cyclodextrin complexes [11]. Encapsulation technology provides a practical approach to enhance the solubility and stability of lipophilic bioactive compounds. Research has demonstrated that the construction of nanoparticles can effectively improve the solubility of active substances, addressing the challenges associated with food processing, transportation, and the preservation of functional substance stability [12]. Ideally, nanoparticles should have an average size of 1 to 100 nm [13]. In pharmaceutical science, particles smaller than 1000 nm are still considered nanoparticles because they exhibit unique physicochemical properties compared to bulk materials [14,15]. Naturally occurring biopolymers, such as polysaccharides and proteins, offer the potential to serve as nanocarriers for encapsulating active substances due to their biocompatibility, low immunogenicity, non-toxicity, and biodegradability [16]. Bletilla striata ((Thμnb.) Reichb. f.), a traditional Chinese medicine, employs dried roots for the treatment of various dermatological conditions, including fissures, edema, burns, abscesses, and freckles. A water-soluble polymer known as Bletilla striata polysaccharides (BSPs) is present in Bletilla striata and is composed of three monosaccharides. BSPs possess exceptional biocompatibility, biodegradability, and immunogenicity, while exhibiting diverse pharmacological effects, including wound healing promotion, antimicrobial activity, anti-aging properties, anti-fibrotic effects, ulcer prevention, antitumor activity, and antiviral properties [17]. BSPs find broad applications in industries such as chemical engineering, pharmaceuticals, and food, where they function as gelling agents, adhesives, and drug carriers, among other roles. Stearic acid-modified BSPs (SA-BSPs), or nanoparticles, are formed by combining Bletilla striata polysaccharides and stearic acid (SA) and serve as effective drug carriers. They can encapsulate poorly soluble or unstable drugs, thereby enhancing drug solubility in water and absorption in the human body. This approach reduces drug toxicity to normal tissues while improving therapeutic effects [18,19].

The innovation addressed in this study focused on the utilization of SA-BSPs as carriers for the preparation of CBD-SA-BSPs copolymer micelles and the evaluation of their advantages in drug delivery. Initially, the hydrophobicity of BSPs was increased through conjugation with SA via ester bonds. Subsequently, CBD-SA-BSPs copolymer micelles were synthesized using an emulsification-solvent evaporation technique. These copolymer micelles underwent comprehensive characterization, including particle size measurement, zeta potential analysis, evaluation of encapsulation efficiency, and determination of drug loading. Furthermore, physicochemical stability and in vitro drug release experiments were conducted on the nanoparticles. The cytotoxicity and apoptosis induced by CBD-SA-BSPs copolymer micelles were evaluated on human liver cancer cell lines (MHCC97H, HCCLM3, HepG2, and Huh7), and in vitro related activity experiments were investigated. Moreover, the use of nanoparticles allowed for achieving high-dose effects with low-dose drug administration, thus minimizing the risk of adverse effects. This study had the potential to address the specific limitations and challenges associated with the practical application of CBD. CBD-SA-BSPs presented new research opportunities in both in vivo and clinical contexts, offering valuable insights into enhancing the bioavailability of CBD in the body and expanding the field of drug delivery systems.

2. Material and method:

2.1. Materials

95% ethanol (CH3OH) was obtained from Sinopharm Chemical Reagent Co., Ltd. Dichloromethane (DCM, CHCCl2) was sourced from Zhengzhou Shuangchen Trading Co., Ltd. and met analytical grade standards. Ultrapure water was prepared in our laboratory. BSPs with a purity of 96% were synthesized in our laboratory. 4-Dimethylaminopyridine and 1-ethyl-3-[3-(dimethylamino)propyl]carbodiimide (EDC) were provided by Shanghai Energy Chemical Co., Ltd. SA was purchased from Sinopharm Chemical Reagent Co., Ltd. in Beijing, China. Cannabidiol with a purity of 99% was also synthesized in our laboratory. Methanol meeting high-performance liquid chromatography (HPLC) grade standards was obtained from Dima Company in the USA. Chromatographic acetonitrile was sourced from Tianjin Baishi Chemical Co., Ltd. Common organic reagents used in the experiment met analytical grade standards, while the reagents utilized for liquid chromatography adhered to chromatographic grade criteria. Ultrapure water was used throughout the study.

2.2. Synthesis of SA-BSPs

SA-BSPs were prepared through the emulsification-solvent evaporation method, with some alterations based on previous literature. In summary, SA (0.9058 g), EDC (0.69 g), and DMPA (0.3818 g) were dissolved in 10 mL of DMSO. Separately, BSPs (2.887 g) were dissolved in 10 mL of DMSO and subjected to magnetic stirring at 30℃ for two hours. Next, the SA reaction solution was slowly added dropwise to the BSP solution under stirring conditions, and the reaction was maintained at 49℃ for 48 hours. After the completion of the reaction, the solution was diluted tenfold with cold ethanol. The resulting precipitate was filtered, collected, and washed three times with 100 mL of ethanol and then with 100 mL of ether. Finally, the precipitate was vacuum-dried at 50℃, yielding 1.52 g of SA-BSPs [19].

2.3. Synthesis of CBD-SA-BSPsNPs

Initially, a 100 mg portion of SA-BSPs was dissolved in 4 mL of DMSO and underwent seven cycles of dialysis against deionized water (0.5 L). The deionized water was changed every 2 hours for the first four cycles and every 8 hours for the remaining three cycles. The rotation speed of the dialysis process was maintained at 100 rpm/min, and the temperature was set at 25℃. Subsequently, the resulting copolymer micelle solution was passed through a 0.45 μm membrane filter and adjusted to a final volume of 50 mL with deionized water. CBD (10 mg, 20 mg, 30 mg) was completely dissolved in 10 mL of a mixed solvent of chloroform and anhydrous ethanol (3:1, v/v). This solution was then slowly added drop by drop into the copolymer micelle solution while under magnetic stirring at 100 rpm for 24 hours. To facilitate the removal of any polymer adhering to the cup wall, 5 mL of deionized water was added, and a vortex mixer was used. The final product was freeze-dried to obtain CBD-SA-BSPs nanomicelles.

2.4. Structural characterization of micelles

2.4.1. 1H NMR spectra

The 1H NMR spectra of each sample were obtained utilizing a nuclear magnetic resonance spectrometer (Avance II-600 MHz, Bruker).

2.4.2. Fourier transform-infrared spectroscopy (FT-IR) analysis

Infrared analysis of the samples was implemented utilizing a Bruker TENSOR 27 Fourier transform infrared spectrometer (Karlsruhe, Germany) in the range of 4000-500 cm-1. The potassium bromide pellet method was employed to process the powder samples. Specifically, approximately 200 mg of potassium bromide powder was blended with 2 mg of the powder sample in an agate mortar until well-ground. The resulting mixture was then compressed into a self-supporting wafer and dried under an infrared lamp for further testing.

2.4.3. Thermogravimetric analysis (TGA)

TGA was implemented utilizing a NETZSCH STA-449 F3 (Bavaria, Germany) instrument in the temperature range of 25 to 950 °C under an ultra-pure nitrogen atmosphere with a flow rate of 25 mL/min. The heating rate was set to 10°C/min.

2.5. HPLC assay

CBD analysis was performed utilizing an HPLC system (Agilent series 1260, USA) equipped with a UV/Vis detector (Agilent G1315C, USA) set to 220 nm for detection. A reverse-phase column (Kromasil C18, AkzoNobel, 250 mm × 4.6 mm, 5 μm) was used for chromatographic separation. The mobile phase consisted of acidified ultrapure water (0.1% formic acid) as solvent A and acidified acetonitrile (0.1% formic acid) as solvent B, with a gradient elution profile: 0 min (30% A), 0-15 min (10% A to 30% A). The flow rate was constant at 1.0 mL/min, and an injection volume of 10 μL was used. The column temperature was maintained at 30°C throughout the analysis.

2.6. Estimation of encapsulation parameters

To determine the encapsulation efficiency (EE%) and drug loading (DL%) of the nanomicelles, a precise amount of nanomicelles was accurately weighed and dissolved in 1 mL of ultrapure water. The resulting solution was then filtered through a 0.22 μm microporous membrane and mixed with an appropriate volume of methanol. This mixture was

subjected to 5 minutes of ultrasonication to disrupt the "core-shell" structure and release the cannabidiol. The solution was further filtered through a 0.22 μm syringe filter before analysis, with an injection volume of 10 μL. This analytical procedure was performed in triplicate, and the obtained peak areas were used to calculate the drug loading (DL%) and encapsulation efficiency (EE%) of the nanomicelles using linear regression equations (Eq. 1 for EE% and Eq. 2 for DL%).

LC="weight of drug in the micelles" /"weight of drug loaded micelles" ×100% (1)

EE=(weight of drug in the micelles)/(weight of the added drug)×100% (2)

2.7. Determination of particle size, polydispersity index (PDI), and potential

The particle size, PDI, and zeta potential of SA-BSPs and CBD-SA-BSPs were determined using a Malvern laser particle size analyzer (Zetasizer Nano ZS90, Malvern Instruments Ltd., Malvern, UK) at 25°C. Three measurements were performed in parallel, and the average value was recorded.

2.8. Stability assays of micelles

2.8.1. In Vitro Drug Release Study

A modified protocol, based on a previously established methodology, was utilized to evaluate the release kinetics of nanomicelles at 37°C. Freeze-dried CBD-loaded micelles were reconstituted in 1 mL of ultrapure water to achieve a CBD concentration of approximately 2 mg/mL. These reconstituted micelles were then encapsulated within dialysis bags with a molecular weight cutoff of 3500 Da and placed in sealed glass containers. Each container contained 20 mL of pH 7.4 phosphate-buffered saline (PBS) solution with 0.5% (w/v) Tween 80. To ensure constant agitation, the sealed containers were placed in a thermostatic incubator shaker operating at an agitation rate of 100 rpm and a temperature of 37°C. Samples were collected at specific intervals (0.25, 0.5, 1, 2, 4, 8, 12, 24, 36, 48, 72, 96, 120, 144, and 168 hours) and CBD release was quantified using the liquid chromatography method described in Section 2.5. The cumulative release rate of CBD was calculated at each time point, facilitating the generation of a release curve for the three different CBD-loaded micelles.

2.8.2. In vitro gastric digestion simulation experiment

CBD-SA-BSPs and CBD with varying loading ratios were individually weighed and fully dissolved in ethanol. The dissolved compounds were then introduced into a simulated saliva solution, and the mixture was agitated in a water bath at 37°C for 2 minutes to simulate oral digestion. After oral digestion, the resulting sample solution was transferred into a dialysis bag with a molecular weight cutoff of 3500 Da. This dialysis bag was immersed in a simulated gastric juice solution and agitated in a water bath at 37°C with a stirring rate of 100 rpm. At 20-minute intervals, 1 mL of the sample was withdrawn, and the drug content was analyzed using the previously established liquid chromatography conditions.

2.8.3. pH stability assay

The pH of the nanoparticle suspension was adjusted in the range of 3 to 10, with subsequent CBD concentration measurements conducted at one-unit intervals of pH.

2.8.4. Thermal stability assay

The nanoparticle suspensions were subjected to heat treatment at 80°C for different durations: 10, 30, 60, and 90 minutes. Following this, rapid cooling to 25°C was carried out, and the resulting variations in CBD concentration were quantified.

2.8.5. Light stability assay

The nanoparticle suspension was transferred into a clear glass vial and exposed to ultraviolet light with a wavelength of 365 nm. CBD concentrations were measured during this exposure.

2.8.6. Storage stability assay

The newly prepared CBD nanoparticle suspensions were stored under three different conditions for 21 days: at 4°C in the dark, at 25°C in the dark, and at 25°C with exposure to light.

2.9 Study on molecular docking between CBD and CB1 receptor

Using core targets for molecular docking, to evaluate their binding potential with CBD. Molecular docking was performed using Autodock Vina 1.5.6 software. The three-dimensional structures of CBD and target proteins were downloaded from PubChem and RCSB PDB databases (http://www.rcsb.org/) respectively (access date: December 16, 2023). After removing water molecules and ligands using PyMol (v2.5.0), the obtained protein structures were imported into AutoDockTools (v1.5.6) to define the active sites of protein molecular docking. The binding ability and stability were evaluated using the calculated binding energy.

2.10. In-vitro cytotoxicity studies

2.10.1. Cell culture

The THLE-2 cells and HCC cell lines (MHCC-97H, HCCLM3, Huh7 and HepG2) used in this study were obtained from the China Center for Type Culture Collection (Shanghai, China). MHCC-97H, HCCLM3 and Huh7 cell lines were cultured in DMEM medium supplemented with 10% fetal bovine serum (FBS) and 1% penicillin-streptomycin, HepG2 cell line was cultured in MEM-ALPHA medium with the same amount of 10% FBS and 1% penicillin-streptomycin, and THLE-2 cells were cultured in BEGM medium. All cell lines were incubated in a humidified incubator at 37°C with 5% CO2.

Prepare the cell suspension and seed the cells in a 96-well plate, about 100 μl per well, with three replicates for each sample. Incubate the plate in a culture incubator for a period of time to allow the cells to adhere or grow stably. Add different concentrations of the test samples to each well of the plate and incubate the plate in a culture incubator for 72 h. Then add 10 μl of CCK-8 solution to each well and incubate the plate in a culture incubator for 4 h to fully develop the color. Measure the absorbance (OD) at 450 nm with an enzyme-linked immunosorbent assay (ELISA) reader and calculate the cell viability or survival rate according to the formula, which is the indicator of cell toxicity.

Cell viability (%) = [A (treated) - A (blank)] / [A (untreated) - A (blank)] × 100

(A (treated) is the OD value of the well with cells, CCK-8 solution and drug solution; A (untreated) is the OD value of the well with cells, CCK-8 solution and no drug solution; A (blank) is the OD value of the well with no cells.)

2.10. 2. Colony formation assay

In the colony formation assay, cells in the logarithmic phase are digested, resuspended in complete medium, and counted. The cell density is adjusted to 3000 cells/mL. Then, 1 mL is added to each well of a 12-well plate, making the number of cells in each well 3000. After shaking, it is left to culture. The day after plating, the 10 mM stock solution of CBD-SA-BSPs is diluted to working solutions of 5 mM and 2.5 mM. Each well (containing 1 mL of medium) is added with 1 μL of the corresponding solvent/compound, making the final concentration of the compound a 1000-fold dilution. That is, each well in the vehicle group is added with 1 μL of DMSO, and each well in the various dose groups is added with 1 μL of a 1000-fold diluted working solution of the compound. After the addition of the drug, the culture is continued. The formation of clones is checked after 7-12 days. When the clone colonies are clearly visible, crystal violet staining is performed.

The steps for crystal violet staining are as follows: remove the medium, wash with PBS to remove the residual medium, add 0.5 mL of 4% paraformaldehyde solution to each well and fix for 1 hour, then pour out the paraformaldehyde solution, wash once with PBS, then add 0.5 mL of 0.2% crystal violet solution to each well and stain for 30 minutes, then collect the crystal violet solution, wash the cell surface with water to remove the floating color, dry and take pictures, and use Image J software to analyze the number of clones.

Colony formation rate = (Number of colonies / Number of seeded cells) × 100%

2.10.3. Apoptosis study

In order to study cell apoptosis, MHCC-97H and HCCLM3 cells in the logarithmic growth phase are treated with a digestive solution. After counting, 1.5-2x105 cells are cultured on a 6-well plate. On the second day of culture, drugs are added and the drugs act for 72 hours. After the action is over, the cells are separated with EDTA-free trypsin and collected into a 1.5 mL EP tube. After washing with PBS, centrifuge at 300g for 5 minutes, remove the supernatant, and add 100 μL of dye prepared with 1×Annexin V Binding Buffer (2.5 μL of Annexin V-FITC Reagent + 2.5 μL of PI Reagent) to gently suspend the cells, and culture in the dark at room temperature for 15-20 minutes. After the culture is over, add 400 μL of diluted 1xAnnexin V Binding Buffer to stop staining, and mix the sample. After filtration, it is detected with a flow cytometer within 1 hour: FSC, SSA, YL2, and FITC channels are selected for flow analysis.

2.10.4. Carboxyfluorescein succinimidyl ester (CFSE) analysis

Cell proliferation rate was assessed through CFSE staining. In short, HCC cells were labeled with 10 mM CFSE (BD Biosciences, Franklin Lakes, NJ, USA) at 37°C for 20 minutes in the dark, followed by two washes with PBS containing 10% FBS (FACS buffer) to remove excess CFSE. Cells were then plated in 6-well plates at a density of 1 × 105 cells per well and incubated for 7 days. Subsequently, HCC cells were detached, washed twice, suspended in FACS buffer, and immediately analyzed using a FACS Calibur flow cytometer (BD Biosciences).

2.11. In Vitro Bioactivity Assays

2.11.1. Hepa1-6 Subcutaneous Tumor Transplantation Experiment

Male C57BL/6J mice, aged 5-6 weeks, were divided into 5 groups, with 8 mice per group. The mice were purchased in advance and acclimatized to the feeding conditions. After one week, subcutaneous tumor inoculation was performed with Hepa1-6 cells. For the evaluation of subcutaneous tumor drug efficacy, the groups were as follows: blank group, solvent group, CBD group (5mg/kg), low-dose CBD-SA-BSPs (3:10) group (5mg/kg), and high-dose CBD-SA-BSPs (3:10)

group (10mg/kg). Starting from the 4th day after tumor inoculation, intraperitoneal injection treatment was performed daily, and tumor volume was tracked and measured every two days. At the end of the experiment, blood was collected from the orbital sinus, and after euthanizing the mice, subcutaneous tumor tissues were weighed and photographed. The tumor inhibition rate was calculated based on the tumor weight[123].

2.11.2 Analysis of Mouse Serum Biochemical Indicators and Histopathology

The mice were restrained and their eyeballs exposed. A capillary tube was inserted into the retro-orbital venous plexus of the mice, and approximately 100 μL of blood was collected into a 1.5 mL EDTA anticoagulant tube. The tube was gently inverted to ensure full contact with the anticoagulant. The collected blood was centrifuged at 1800 g for 10 minutes in a 4°C centrifuge to obtain the upper serum layer. The levels of pro-inflammatory cytokines IL-2, IL-6, and TNF-α in the mouse serum were determined using an ELISA kit. The collected mouse liver and kidney tissues were immersed in 10% formalin buffer for 24 hours for fixation. After fixation, the tissues were embedded in paraffin, and the embedded tissue blocks were cut into thin sections of 5 μm thickness. The sections were then stained with hematoxylin and eosin (H&E) and made into H&E slides. The slides were observed under an Olympus IX83 microscope, and a histopathological evaluation of the mouse liver tissue was performed.

2.12. Statistical analyses

Data are presented as mean ± standard deviation (SD) of replicate measurements from independent assays (n=3). Statistical significance was assessed using appropriate tests, including one-way analysis of variance (ANOVA) and Student's t-test. GraphPad Prism 9 software was utilized for all statistical analyses, with significance set at p-values < 0.05.

3. Results and Discussion:

3.1. Structural and property analysis

The chemical composition of SA, BSPs, and SA-BSPs dissolved in DMSO-d6 was elucidated in the 1H-NMR spectra depicted in Fig. 1. The carboxyl (-COOH) proton signal at δ8.69 ppm was attributed to the esterification reaction between SA and BSPs [20]. The methyl (-CH3) and methylene (-CH2) protons of SA, evidenced by the peaks at δ3.36 ppm and δ3.03 ppm, respectively, indicated their linkage to the sugar ring of BSPs. Moreover, the presence of peaks at δ7.23 ppm, δ6.69 ppm, δ2.68 ppm, δ1.46 ppm, and δ0.86 indicated the phenyl and hydroxyl proton signals of BSPs, confirming the preservation of these functional groups following SA modification. Additionally, the peaks at δ5.33 ppm, δ5.08 ppm, δ4.44 ppm, δ3.82 ppm, δ2.50 ppm, and δ2.05~δ1.95 ppm, representing the anomeric and sugar ring proton signals of BSPs, provided evidence of their interaction with SA [18]. Taken together, these data conclusively demonstrate that the modification of BSPs by SA involved a chemical reaction rather than a mere physical mixture.

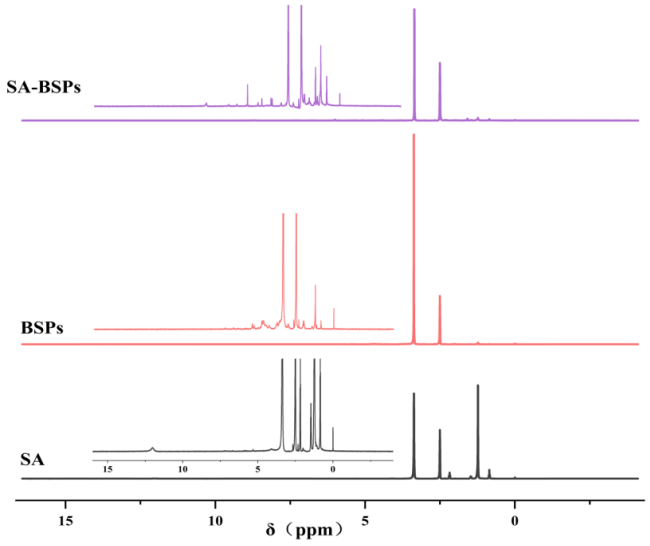

Fig. 1. 1H-NMR spectra of SA, BSPs, and SA-BSPs.

3.2. FT-IR spectra

Fig. 2 presents the FT-IR spectra of SA, BSPs, SA-BSPs, CBD, and CBD-SA-BSPs. The FT-IR spectrum of CBD-SA-BSPs showed characteristic peaks corresponding to both SA-BSPs and CBD, indicating the successful synthesis of SA-BSPs and the encapsulation of CBD. The presence of peaks at 3419.63 cm-1, corresponding to the polysaccharides, was observed in the infrared spectroscopic data of SA-BSPs. A slightly weaker peak at 3419.63 cm-1 for the hydroxyl stretching vibration suggested the partial substitution of hydroxyl groups in the polysaccharide molecules by stearic acid, forming ester bonds [20]. Peaks at 2930.11 cm-1 and 2853.49 cm-1, indicative of the symmetric and asymmetric stretching vibrations of methyl and methylene groups in SA, were also identified. Furthermore, peaks at 1448.06 cm-1 and 1214.73 cm-1, representing the symmetric and asymmetric stretching vibrations of the carbonyl group in the ester bonds, were observed in SA-BSPs, demonstrating interactions between stearic acid's ester bonds and the polysaccharide's carbonyl groups, resulting in a stable structure. These findings suggested that SA primarily modified BSPs through esterification reactions, introducing long-chain fatty acid groups onto the terminal or side chains of the polysaccharide molecules [21]. Additionally, the FT-IR spectrum of CBD-SA-BSPs exhibited a reduction in the original benzene ring absorption peak of CBD at 1514.13 cm-1, indicating the substitution reactions of hydrophilic functional groups, like hydroxyl groups in SA-BSPs, on the benzene ring of CBD. This substitution reaction made CBD-SA-BSPs more hydrophilic, enhancing their water solubility and influencing thermal analysis parameters such as volatility and mass loss.

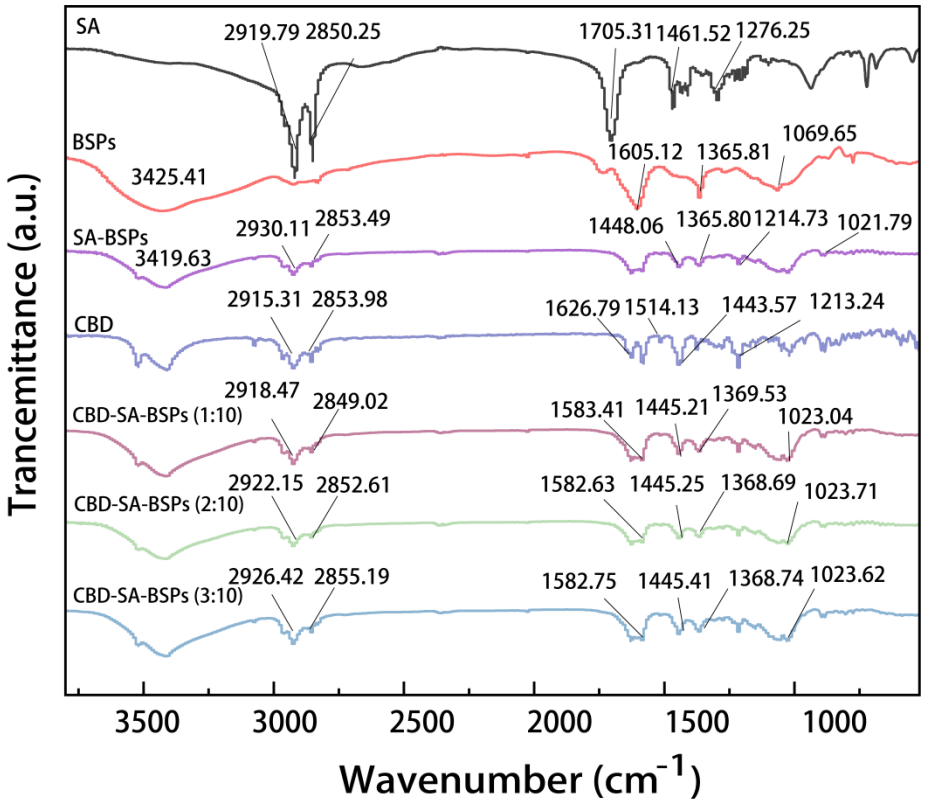

Fig. 2. Fourier transform infrared spectral analysis.

3.3. Thermogravimetric analysis

Fig. 3 presents the thermogravimetric analysis of SA, BSPs, SA-BSPs, CBD, and CBD-SA-BSPs, along with a detailed comparative evaluation of their mass loss profiles. The results revealed significant differences in the patterns of mass loss between BSPs and the individual components of SA or BSPs. SA exhibited a boiling point of approximately 310°C, while BSPs displayed a slightly higher boiling point of around 320°C [22]. Conversely, SA-BSPs demonstrated a notably elevated boiling point of approximately 475°C. CBD had a boiling point of approximately 325°C, whereas CBD-SA-BSPs exhibited a higher boiling point of approximately 440°C. These findings suggest that the modification of BSPs with SA resulted in distinctive thermal stability compared to SA or BSPs alone [23]. The interaction between SA and BSPs led to the formation of novel compounds through chemical bonding. Furthermore, the inclusion of CBD in SA-BSPs resulted in compounds with altered thermal properties. As a result, distinct temperature-dependent behaviors were observed during the thermal analysis of SA-BSPs and CBD-SA-BSPs.

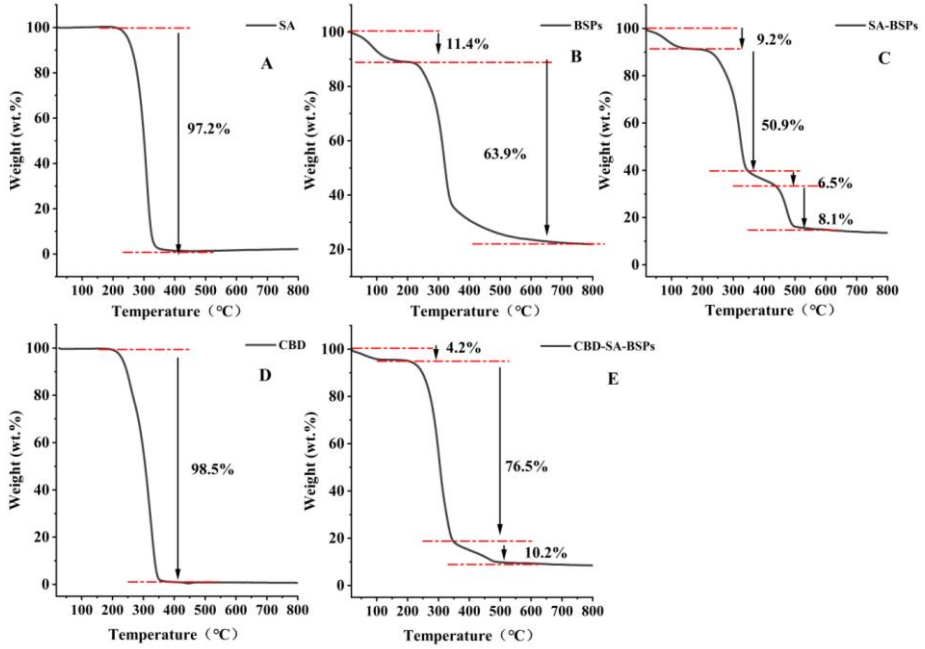

Fig. 3. TGA curves for SA (a), BSPs (b), SA-BSPs (c), CBD (d) and CBD-SA-BSPs(e).

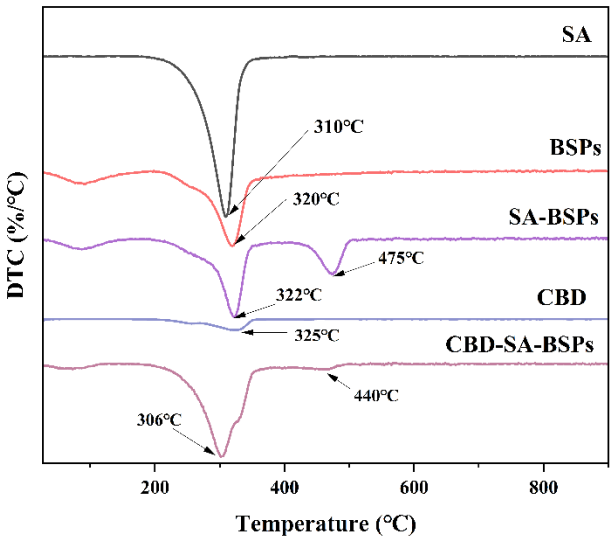

Fig. 4. DTC curves for SA, BSPs, SA-BSPs, CBD, and CBD-SA-BSPs.

3.4. HPLC analysis

Fig. 5 displays the chromatograms of cannabidiol standards, drug carriers, and their constituents. Under consistent chromatographic conditions, the respective samples were prepared and underwent a 10 μL injection into the HPLC instrument. The experimental findings revealed that cannabidiol exhibited a retention time of approximately 9 minutes, demonstrating well-defined peak symmetry and minimal interference from excipients and other components. The peak area (A) was recorded as previously described, establishing a standard curve to correlate the peak area (A) with the mass concentration (C, μg/mL), as presented in Figure 5. The linear equation describing this relationship was y = 84509x

+ 50.72, with a correlation coefficient (r) of 0.9997. These results established a robust linear correlation between the mass concentration of cannabidiol and the corresponding peak area within the effective range of 4 to 100 μg/mL [24,25].

The liquid chromatography profiles revealed that cannabidiol eluted at 9.08 minutes, while CBD-SA-BSPs exhibited an elution time of 9.17 minutes. This discrepancy in elution times suggested a chemical reaction occurring within the complex. Further analysis indicated that a substitution reaction occurred between cannabidiol and SA-BSPs, wherein hydroxyl groups in SA-BSPs replaced hydrogen atoms on the benzene ring of cannabidiol. As a result, the molecular structure and polarity of cannabidiol were altered. This substitution increased the molecular mass of cannabidiol, leading to a prolonged retention time on the chromatographic column and delayed elution compared to unreacted cannabidiol. Additionally, the substitution reaction enhanced the hydrophilicity of cannabidiol, reducing its distribution coefficient in a non-polar mobile phase [26]. Consequently, the elution time for CBD-SA-BSPs was notably delayed compared to CBD alone.

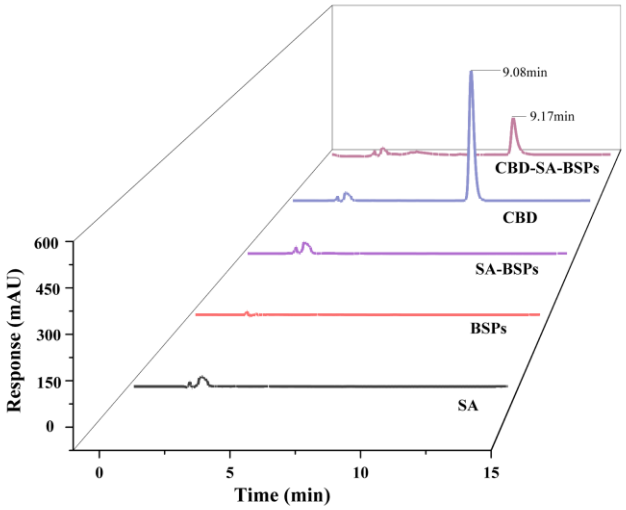

Fig. 5. Chromatogram of cannabidiol standard, drug carrier, and its components.

3.5. Encapsulation efficiency and loading capacity

Fig. 6 illustrates the different parameters of SA-BSPs and CBD-SA-BSPs, which include particle size, encapsulation efficiency, and drug loading [27]. As the carrier/drug (w/w) ratio increased, the particle size of the micelles gradually expanded, accompanied by an increase in the Polydispersity Index (PDI) and zeta potential. Meanwhile, drug loading and encapsulation efficiency remained relatively consistent. Both CBD and SA-BSPs played a role in influencing the particle size of the micelles. An increment in CBD content led to increased hydrophobicity in the micelles, resulting in a larger micelle size. The preparation method and conditions influenced the PDI. In this study, micelles were prepared using an emulsification-solvent evaporation method, which could have led to incomplete encapsulation or dissolution

of certain CBD or SA-BSPs, leading to variations in micelle size. Furthermore, the zeta potential was influenced by the surface composition of the micelles and the external pH environment. The zeta potential was approximately -5.34 mV±0.19mV at a carrier/drug ratio of 10:1, but decreased to approximately -8.79 mV±0.21mV at a ratio of 10:3. Drug loading was influenced by the hydrophobicity and contents of CBD and SA-BSPs. Increasing CBD content resulted in higher drug loading. At a carrier/drug ratio of 10:1, drug loading was approximately 7.41%±0.14%, while at a ratio of 10:3, it increased to approximately 8.94%±0.11%. Due to the emulsification-solvent evaporation method used for micelle preparation and the strong non-covalent binding interactions between CBD and SA-BSPs, the encapsulation efficiency remained consistently high across all ratios. Specifically, at a carrier/drug ratio of 10:1, an encapsulation efficiency of approximately 87.71%±0.24 was achieved, which increased to approximately 92.07%±0.18 at a ratio of 10:3.

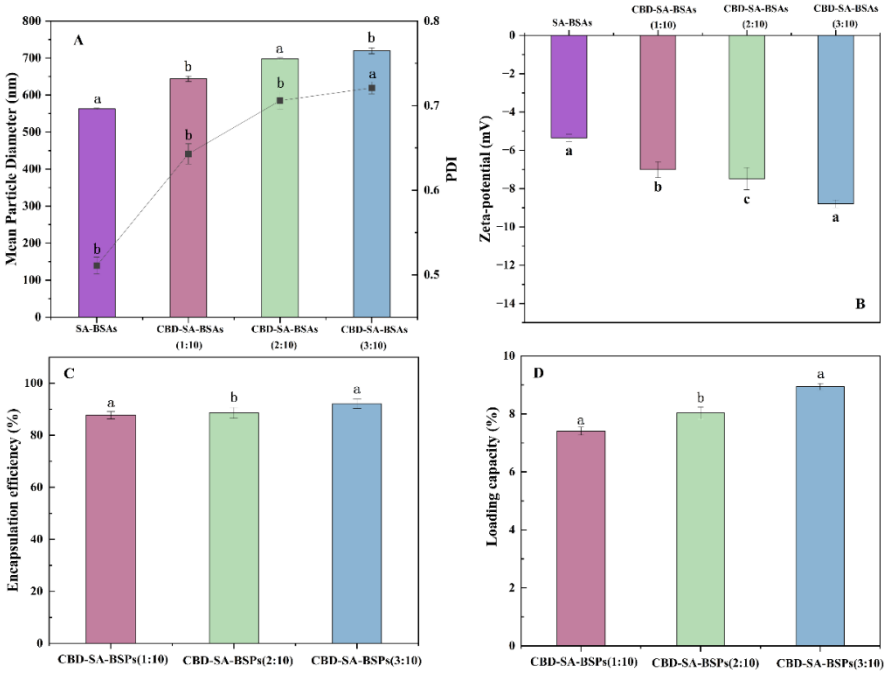

Fig. 6. Mean particle diameter, polydispersity index (PDI) (a), zeta-potential (b), encapsulation efficiency (c), and Loading capacity(d).

3.6. In vitro gastric digestion simulation and drug release study

In vitro gastric digestion simulation experiments revealed that after 2 hours of simulated gastric fluid digestion, the CBD-SA-BSPs (1:10), CBD-SA-BSPs (2:10), and CBD-SA-BSPs (3:10) reached final concentrations of 39.72±3.62 μg/mL, 45.44±3.11 μg/mL, and 50.24±3.02 μg/mL, respectively. In comparison, the concentration of CBD alone was 221.23±3.7 μg/mL. The controlled release of encapsulated cannabidiol facilitated a slower and sustained drug release within the body (Fig. 7a) [28]. Considering the low solubility of cannabidiol in water (0.1 μg/mL), a dialysis medium consisting of a phosphate buffer solution (pH 7.4) with 0.5% Tween 80 was used to meet the precipitation conditions. In vitro drug

release studies showed that within one week, the cumulative release rates of cannabidiol-loaded micelles were 37.51%±0.63%, 38.79%±0.5%, and 40.21%±0.62%, respectively (Fig. 7b). These results indicate excellent sustained release performance of the cannabidiol nanomicelles, highlighting their potential for prolonging the circulation time of cannabidiol in the body [29].

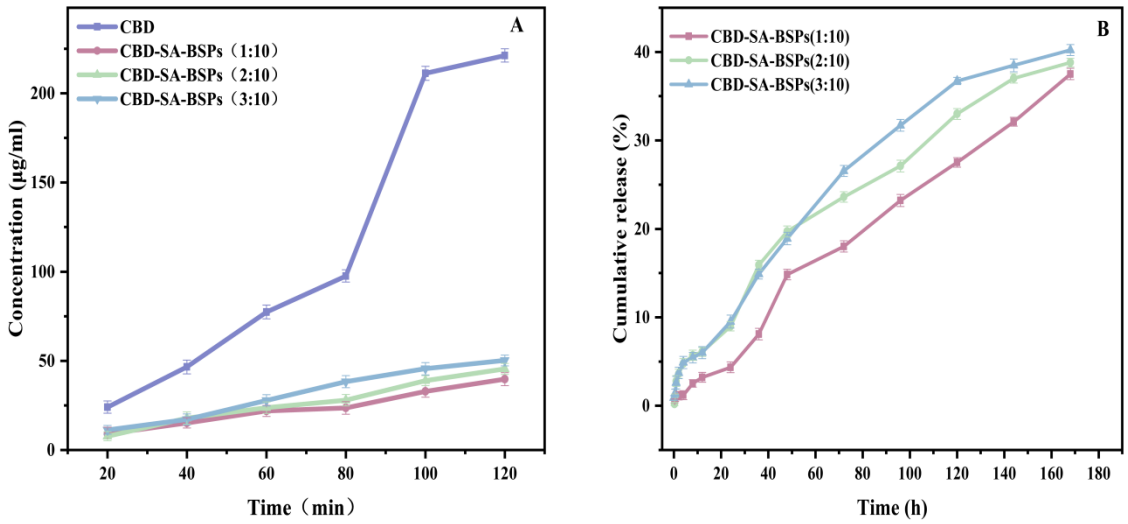

Fig. 7. Vitro gastric digestion simulation (a) and drug release study (b).

3.7. Study on the physicochemical stability of nanoparticles

The stability of CBD nanoparticles was investigated under various conditions, including pH, temperature, light exposure, and storage. pH was identified as a critical factor influencing the stability and bioavailability of CBD [30,31]. In both acidic and alkaline environments, CBD was susceptible to chemical conversion or oxidative degradation, resulting in the loss of CBD or a decrease in its activity. The impact of pH on CBD depended on the choice of carrier material and the mode of administration. Biopolymers, such as proteins or polysaccharides, when used as carrier materials, can enhance the pH stability of CBD. This enhancement is attributed to their ability to form core-shell structured nanoparticles, providing a protective shield for CBD against environmental factors. Empirical investigations have shown that, under acidic conditions, CBD concentrations decrease due to its conversion into Δ9-THC or similar compounds, leading to CBD loss or degradation [32]. Similarly, SA-BSPs nanoparticles displayed limited stability under acidic conditions. Under neutral conditions, CBD concentrations increased as both CBD and SA-BSPs nanoparticles remained stable, ensuring the preservation of CBD encapsulation. Furthermore, SA-BSPs nanoparticles demonstrated notable drug loading and encapsulation efficiency, enhancing CBD solubility at this pH level. Under alkaline conditions, CBD concentrations were slightly lower than those under neutral conditions, as CBD may undergo oxidation, forming

hydroxyquinone or other byproducts, consequently reducing CBD concentration. SA-BSPs nanoparticles exhibited relatively stable behavior under alkaline conditions, thereby maintaining CBD encapsulation [33].

During the heat stability experiment, it was found that the concentration of CBD within SA-BSPs nanoparticles decreased with increasing heating time, indicating the nanoparticle's instability at elevated temperatures, leading to CBD loss or degradation. However, even after a 90-minute heating period at 80°C, a CBD concentration of over 200 μg/mL was maintained, demonstrating the notable heat stability of the material and its ability to protect CBD from damage caused by high temperatures. Previous research has shown that CBD is highly prone to photodegradation [10]. The outer shell of CBD-SA-BSPs nanoparticles acted as a protective barrier against light, resulting in a reduced rate of CBD release. Following a 90-minute exposure to 365 nm ultraviolet light, the CBD concentration remained above 300 μg/mL, highlighting the substantial photostability of the material and its ability to safeguard CBD from the harmful effects of ultraviolet light. Furthermore, the storage stability of CBD-SA-BSPs nanoparticles was evaluated, and no phase separation or precipitation was observed during the testing period. After 21 days of storage, the CBD concentrations ranked as follows: 4°C/darkness > 25°C/darkness > 25°C/light. Greater stability was observed at 4°C compared to 25°C, and exposure to light significantly compromised CBD storage [31]. Therefore, it is recommended to store the nanoparticles in optimal conditions (in the dark and at refrigerated temperatures) to extend the shelf life of CBD formulations.

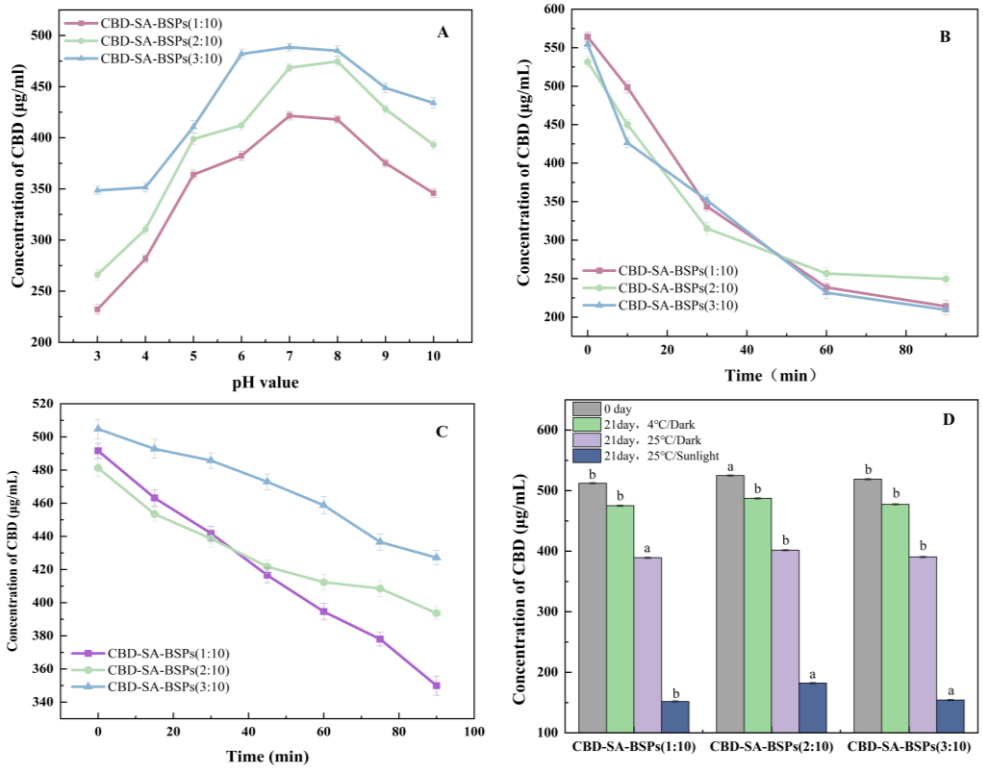

Fig. 8. Effect of pH on CBD concentration of nanoparticles (a), the effect of thermal treatment on CBD concentration of nanoparticles (b), the effect of UV light irradiation on CBD concentration of Nanoparticles (c), the influence of storage period on CBD concentration of nanoparticles (d).

3.8. Study on molecular docking between CBD and CB1 receptor

CB1 receptor is a target of cannabinoids, which can regulate various physiological functions. Studies have found that the expression level of CB1 receptor in hepatocellular carcinoma tissues is higher than that in normal liver tissues, which may be related to the occurrence and development of hepatocellular carcinoma [34]. CB1 can affect some cell signaling pathways, one of which is the IL-1β/IL-1RI/β-catenin signaling pathway. The IL-1β/IL-1RI/β-catenin signaling pathway is a complex network involving various cytokines and proteins, which plays an important role in the tumorigenesis, development and metastasis. Akt protein is a kinase, which can phosphorylate and activate other proteins, promoting cell growth, survival and migration. Akt protein plays a key role in the IL-1β/IL-1RI/β-catenin signaling pathway, which can phosphorylate and inhibit the degradation of β-catenin. β-catenin is a transcription factor, which can regulate the expression of some genes, affecting cell adhesion, proliferation and differentiation. β-catenin usually binds to E-cadherin protein on the cell membrane, maintaining cell stability and polarity. When β-catenin is phosphorylated, it dissociates from E-cadherin protein, enters the nucleus, and activates some genes that promote tumor development. CBD binds to CB1 receptor, reduces Akt protein phosphorylation, thereby inhibits the IL-1β/IL-1RI/β-catenin signaling pathway, prevents β-catenin nuclear translocation, reduces the levels of related genes and proteins in the pathway, increases E-cadherin protein and β-catenin, thereby restores the tumor cell phenotype, makes malignant tumor cells sensitive to conventional treatment methods, and improves the efficacy of chemotherapeutic drugs with resistance [35]. Protein Cannabinoid receptor 1 P21554 is a G protein-coupled receptor, which can be activated by endocannabinoids (EC) or exogenous cannabinoids (such as THC), thereby regulating various physiological and pathological processes. 7wv9 and 7v3z are the crystal structure codes of P21554, representing the forms of P21554 binding to two different ligands. Molecular docking is a technical method to simulate the interaction between ligand small molecules and receptor biomacromolecules, which can predict the binding mode and binding energy between them, and screen out compounds that may have biological activity. CBD and 7wv9, 7v3z were docked to explore whether CBD can interact with different ligand forms of P21554, thereby affecting the function of P21554, and then regulating the process of cell apoptosis. CBD can induce apoptosis of tumor cells through various pathways, one of which is to up-regulate the expression of P21554, and enhance the sensitivity of tumor cells to TRAIL [36]. For molecular docking, the binding energy between compounds and proteins less than 0 can be regarded as an indication of spontaneous binding, and the

binding energy less than -7 kJ/mol is regarded as a more stable binding mode. Lower binding energy means more stable binding. The molecular docking binding energy of CBD with key targets are as follows: CB1 (7wv9) = -7.5 kJ/mol, CB1 (7v3z) = -6.3 kJ/mol. The binding energy between CBD and target proteins was evaluated by hydrogen bonds, bond length, CBD and amino acid residues, and 3D interactions (Figure 9). The molecular docking results showed that CBD has a strong binding ability with CB1.

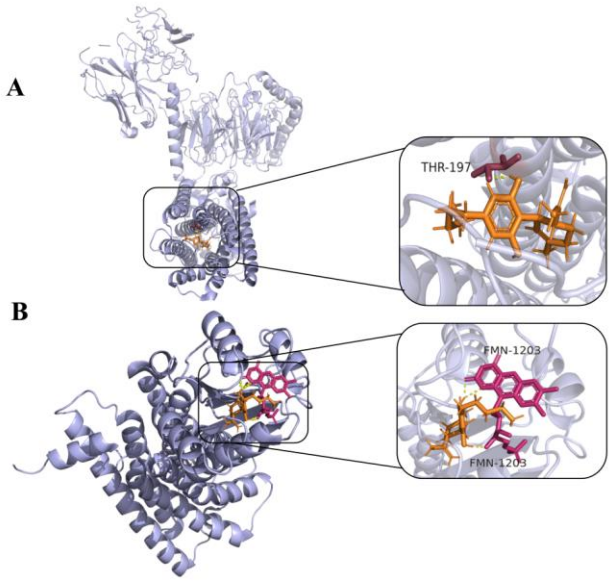

Fig. 9. Molecular docking of CBD with CB1 receptor. (A) Docking diagram of CBD and 7wv9, (B) Docking diagram of CBD and 7v3z.

3.9 THLE-2 cell toxicity assay

The human immortalized liver cell THLE-2 is a normal human liver cell line, which is often used for studying liver-related diseases and drug effects [37]. The purpose of this experiment was to investigate the toxicity of CBD, SA-BSPs copolymer micelles and CBD-SA-BSPs nanoparticles on THLE-2 cells by using CCK-8 method, to evaluate their safety and biocompatibility as drug carriers. As shown in Figure 10, when the concentration of SA-BSPs copolymer micelles was in the range of 0~20 μg/mL, the cell viability of THLE-2 cells was above 90%, indicating that the micelles could be safely used as drug carriers. As the concentration of micelles increased from 2.5 μg/mL to 20 μg/mL, the cell survival rate decreased from 103.79%±5.07% to 95.49%±2.54%. The literature research results showed that SA-BSPs copolymer micelles had no toxicity and hemolysis below 1 mg/ mL [18]. Therefore, SA-BSPs copolymer micelles were safe and biocompatible.

CBD and CBD-SA-BSPs nanoparticles, at the concentration of 20 μg/mL, had the cell viability of THLE-2 cells as follows: CBD was 102.14%±2.54%; CBD-SA-BSPs (1:10) was 91.06%±0.23%; CBD-SA-BSPs (2:10) was 93.25%±2.40%;

CBD-SA-BSPs (3:10) was 93.49% ±3.30%, respectively, with the cell viability above 90%. The research results showed that the samples had no significant effect on the proliferation of normal liver cells THLE-2.

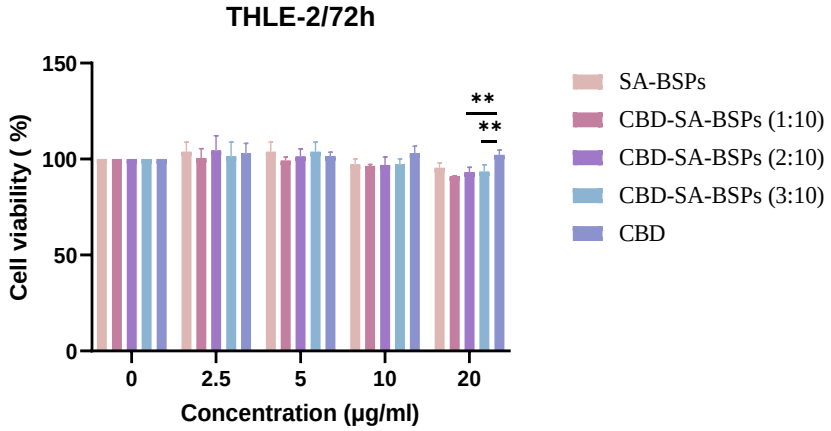

Fig. 10. In vitro study of THLE-2 cells induced by copolymer micelles of SA-BSPs, CBD and CBD-SA-BSPS at different loading ratios.

3.10. Cell proliferation/viability assay

To evaluate the growth-inhibitory effects of CBD-SA-BSPs nanomicelles on liver cancer cells, CCK-8 assays were performed to assess their impact on four liver cancer cell lines (MHCC97H, HCCLM3, HepG2, Huh7) at different concentrations. The results indicated a dose-dependent reduction in the viability of liver cancer cells when exposed to CBD-SA-BSPs nanomicelles. Fig. 11 shows a significant dose-dependent inhibitory effect in MHCC97H, HCCLM3, HepG2, and Huh7 cells within the concentration range of 0 to 20 μg/mL. Both CBD and CBD-SA-BSPs copolymer micelles exhibited similar antitumor activity across the four cancer cell lines. The SA-BSPs copolymer micelles demonstrated remarkable biocompatibility, causing minimal impact on cell proliferation. At a concentration of 20 μg/mL, the antitumor activities against MHCC97H, HepG2, HCCLM3, and Huh7 cells were as follows: CBD: 17.98%±2.79%, 79.26%±0.43%, 77.83%±0.16%, and -3.10%±3.84%, respectively; CBD-SA-BSPs (1:10): 18.1%±1.48%, 80.94%±0.3%, 74.84%±0.29%, and 7.4%±1.72%, respectively; CBD-SA-BSPs (2:10): 26.16%±0.81%, 85.22%±0.75%, 81.13%±0.62%, and 9.06%±1.57%, respectively; and CBD-SA-BSPs (3:10): 28.21%±2.29%, 85.35%±0.64%, 81.57%±0.57%, and 18.1%±0.84%, respectively. Notably, the SA-BSPs copolymer micelles without any drug payload exhibited antitumor activity exclusively against HepG2 and HCCLM3 cells, with rates of 11.73%±5.65% and 6.12%±0.11%, respectively. The growth of cancer cells was only inhibited by SA-BSPs, and the biocompatibility of the blank SA-BSPs copolymer micelles was maintained, possibly due to the inherent antitumor activity of SA-BSPs [38]. These results emphasized the strong cytotoxic effects of CBD-SA-BSPs copolymer micelles on tumor cells, particularly the CBD-SA-BSPs (3:10) micelles, which displayed superior antitumor activity compared to CBD alone. These differences were found

to be statistically significant. One possible reason is that the micelles, due to their high retention and permeability, can be efficiently internalized by cancer cells through endocytosis, facilitating drug uptake near the desired target site [39]. Cancer cells possess specific endocytic properties, which enable them to internalize CBD-SA-BSPs copolymer micelles, leading to increased drug concentrations in close proximity to the site of action [40]. Furthermore, the prolonged and gradual release of CBD from CBD-SA-BSPs copolymer micelles may contribute to this effect. However, future investigations are necessary to fully understand this phenomenon. Based on these findings, the CBD-SA-BSPs (3:10) micelles were chosen for subsequent cell phenotype experiments.

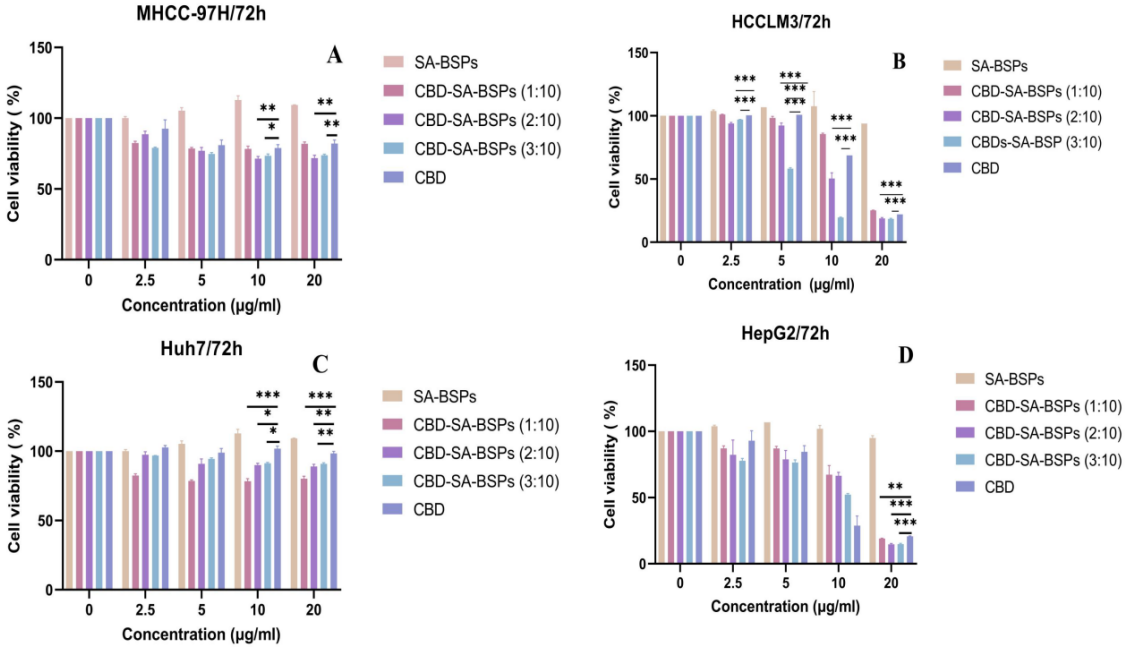

Fig. 11. In vitro study of the antitumor activity of SA-BSPs, CBD, and CBD-SA-BSPs copolymer micelles at varying drug loading ratios. (a) Inhibition of 97H cell growth, (b) Inhibition of HepG2 cell growth, (c) Suppression of LM3 cell proliferation, and (d) Inhibition of Huh7 cell growth.(* means $p<0.05$, ** means $p<0.01$, *** means $p<0.001$)

3.11. Colony formation assay

The colony formation assay results revealed a significant decrease in the number of colonies formed in the treatment group compared to the control group (Fig. 12). As the duration of cell culture increased, the inhibition of clone formation for MHCC-97H and HCCLM3 cells at a concentration of 20 μg/mL was 26.99%±6.87% and 26.81%±4.2%, respectively. The proliferation rate of cells in the CBD-SA-BSPs group was remarkably lower than that in the control group, and this difference was statistically significant ($P < 0.001$). In conclusion, these findings indicate that CBD-SA-BSPs (3:10) effectively suppressed the proliferation and reduced the viability of MHCC-97H and HCCLM3 cells [41,42].

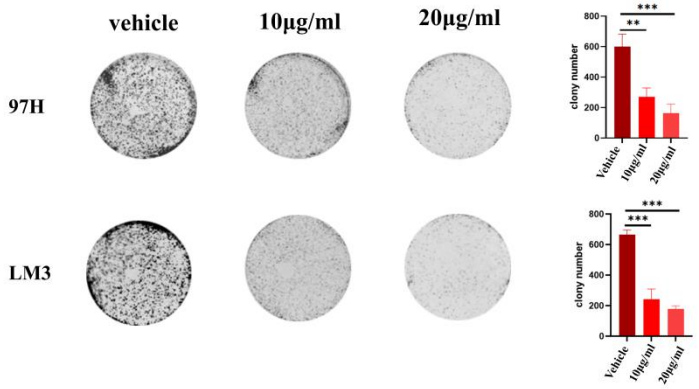

Fig. 12. Inhibition of colony formation in 97H and LM3 Cells by CBD-SA-BSPs (3:10).

3.12. Apoptosis study

The impact of CBD-SA-BSPs on inducing apoptosis in liver cancer cells was assessed using a PI/Annexin V double staining assay [43]. The results demonstrated a dose-dependent increase in the percentage of both early and late apoptotic cells in MHCC-97H and HCCLM3 cells when exposed to increasing concentrations of CBD-SA-BSPs (3:10). At a concentration of 20 μg/mL of CBD-SA-BSPs (3:10), the apoptosis rates for MHCC-97H and HCCLM3 cells were 43.8%±2.88% and 36.57%±4.67%, respectively.

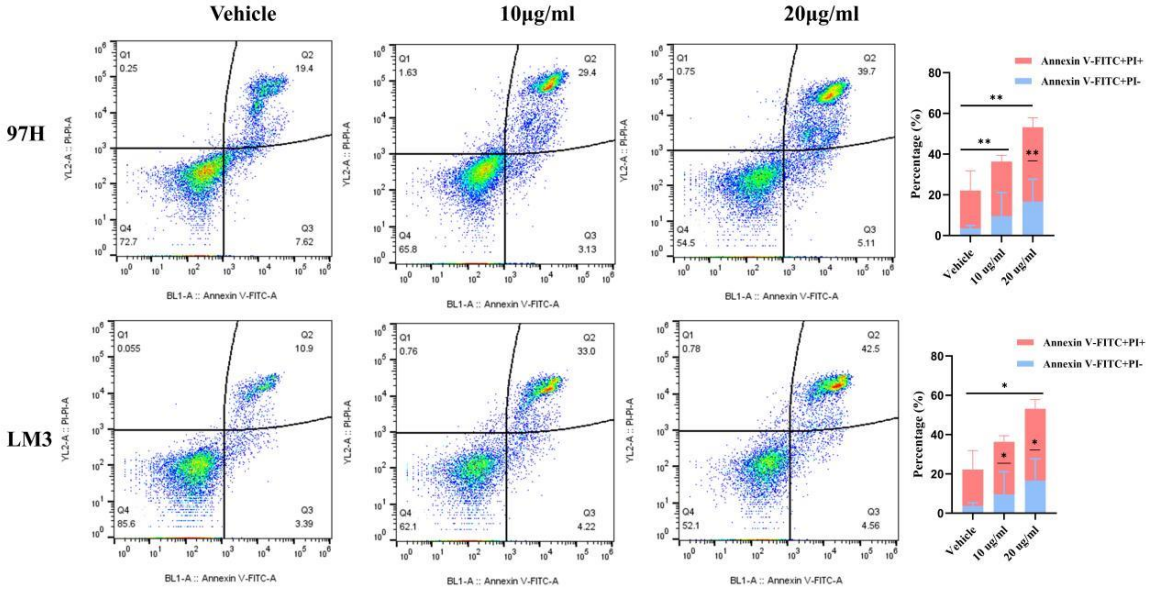

Fig. 13. Induction of Apoptosis in 97H and LM3 by CBD-SA-BSPs (3:10).

3.13. CFSE assay for detecting cell proliferation

The findings obtained from the CFSE assay validated the results mentioned earlier. Treatment with CBD-SA-BSPs led to an increase in the average fluorescence intensity of CFSE in both MHCC-97H and HCCLM3 cells compared to the

control group. Additionally, as the drug concentration increased, the average fluorescence intensity of CFSE gradually rose (Fig. 14). At a concentration of 20 μg/mL of CBD-SA-BSPs (3:10), the proliferation inhibition rate was 59.79%±3.49% for MHCC-97H and 69.82%±2.03% for HCCLM3. These outcomes demonstrated that CBD-SA-BSPs (3:10) reduced the division rate in MHCC-97H and HCCLM3 cells, effectively inhibiting their proliferation.

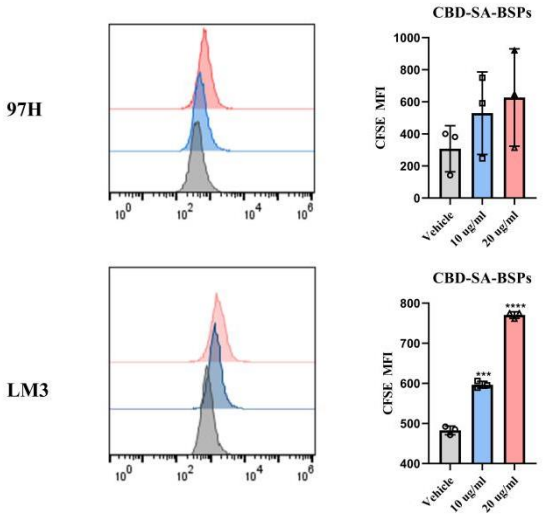

Fig. 14. Inhibition of Proliferation in 97H and LM3 by CBD-SA-BSPs (3:10)

3.14. The Inhibitory Effect of CBD-SA-BSPs on the Proliferation of Hepa1-6 Cells in Mice

A subcutaneous tumor model of Hepa1-6 was established, and tumor-bearing mice were administered with 5mg/kg CBD and 5mg/kg and 10mg/kg CBD-SA-BSPs for 21 consecutive days. The tumor volume was tracked and measured. As shown in Fig. 15, compared with the solvent control, both 5mg/kg CBD-SA-BSPs and 10mg/kg CBD-SA-BSPs significantly inhibited the growth of subcutaneous tumors of Hepa1-6. At the end of the experiment, the subcutaneous tumors of the mice were dissected and weighed for analysis. The results showed that the tumor inhibition rate of the 5mg/kg CBD group, 5mg/kg CBD-SA-BSPs (3:10) group and 10mg/kg CBD-SA-BSPs (3:10) group separately were 35.28%, 46.94% and 72.83%. The results of mouse weight monitoring showed that there was no significant difference in the weight of mice in different dosage groups and the solvent group, and no other obvious toxic reactions were observed, verifying the safety of CBD-SA-BSPs.

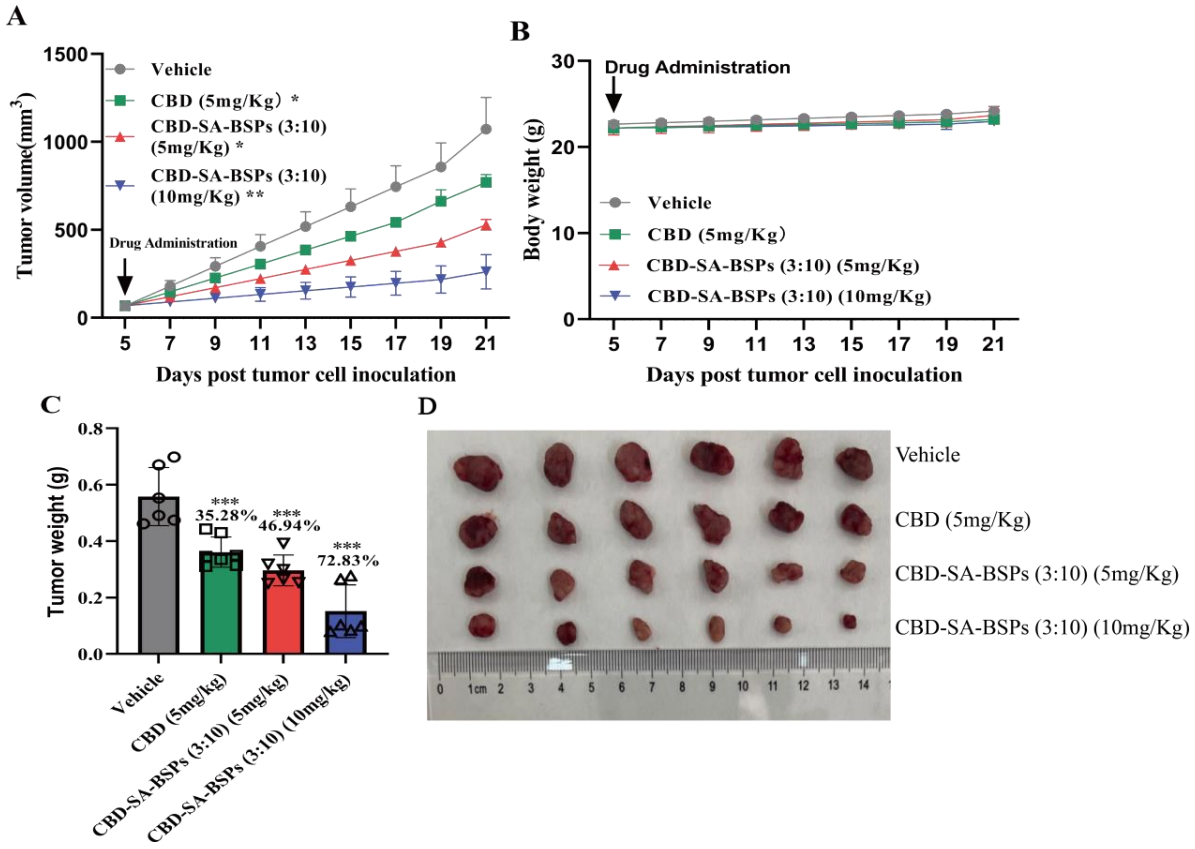

Fig. 15. Inhibition of subcutaneous tumorigenesis of Hepa1-6 by CBD-SA-BSPs. (A) Growth curve graphs of subcutaneous tumors in each group of mice. (B) Body weight changes in each group of mice post-administration. (C) Statistical graph of tumor weight and tumor inhibition rate for each group's subcutaneous tumors. (D) Photographs of the excised subcutaneous tumors at the end of the experiment. All results were analyzed using a t-test with GraphPad Prism 9.0.0. Data are presented as mean ± SD, n = 6, *P < 0.05, **P < 0.01.

3.15. CBD-SA-BSPs Reduce the Levels of Pro-inflammatory Cytokines in Mouse Hepatocellular Carcinoma Cells

Compared with the model group, the levels of pro-inflammatory cytokines IL-2, IL-6, and TNF-α in the serum of mice in the three drug-administered groups were significantly reduced, suggesting that the drug may exert its anti-hepatocarcinoma effect by regulating the levels of these cytokines (Fig. 16). To further verify the safety of CBD-SA-BSPs in vivo, liver and kidney tissue sections and H&E staining were performed on mice after the treatment ended. Microscopic examination results showed that there were no significant differences in the H&E staining results of liver and kidney tissues of mice in each experimental group compared with the control group, indicating that intraperitoneal injection of CBD-SA-BSPs does not cause toxic side effects. The polymer constructed in this study has excellent biocompatibility and safety.

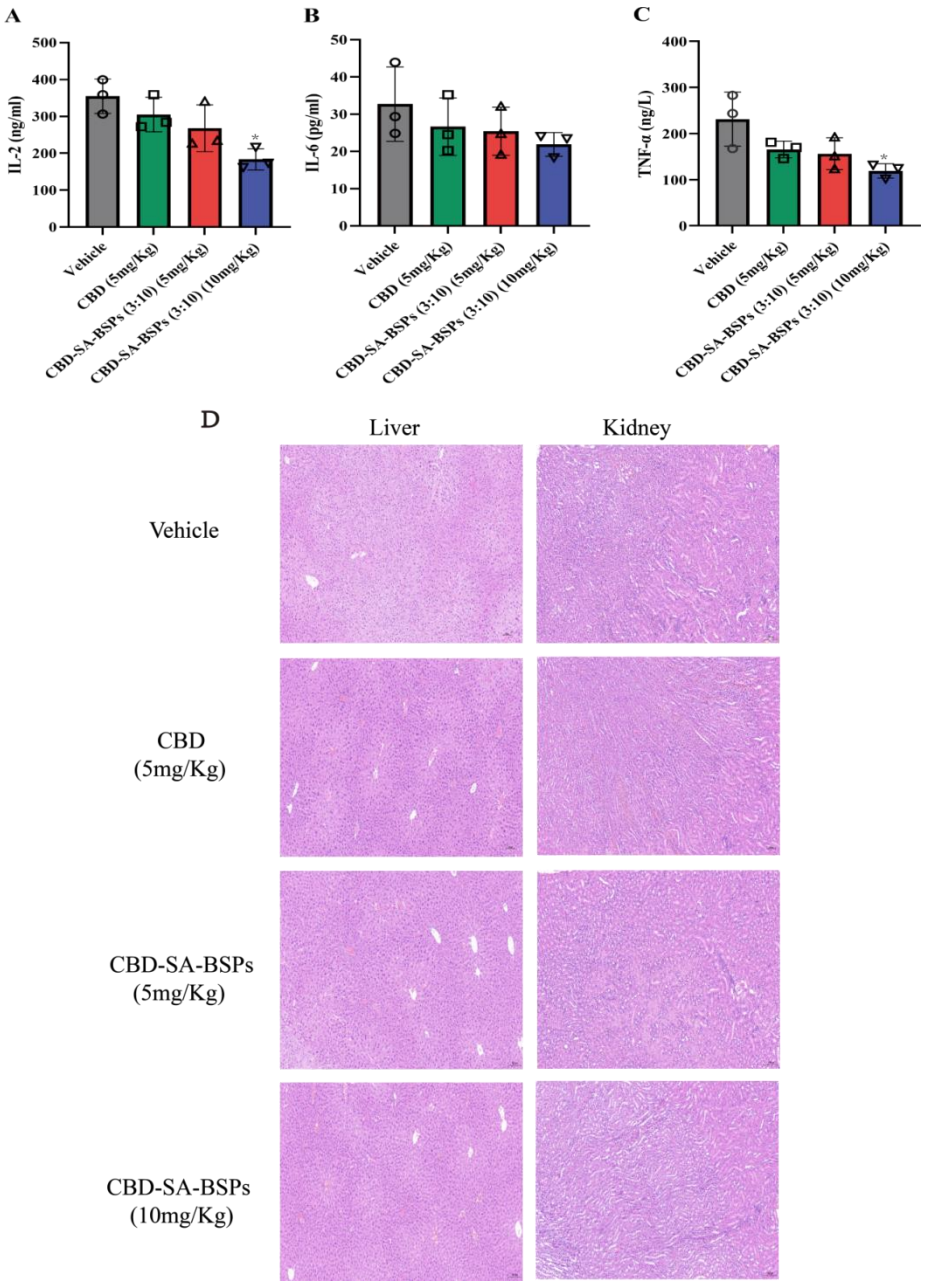

Fig. 16. CBD-SA-BSPs effectively mitigate the action of cancer inflammatory cytokines.Levels of (A) IL-2; (B) IL-6; (C) TNF-α in mouse serum and H&E Staining of Liver and Kidney Tissues in Various Experimental Mouse Groups (*P < 0.05)

4. Conclusion:

In this article, we have described the preparation of nanomicelles by utilizing SA-BSPs as carriers for encapsulating CBD. The stability and release behavior of these nanomicelles under different conditions were thoroughly investigated, demonstrating their exceptional resistance to digestive processes and prolonged release characteristics. These attributes contributed to the enhanced bioavailability of CBD. The nanomicelles exhibited high levels of encapsulation efficiency,

drug loading capacity, stability, and sustained release performance, along with significant anti-hepatocellular carcinoma (HCC) activity. The utilization of these nanomicelles holds great promise for improving the solubility, bioavailability, and antitumor efficacy of CBD. SA-BSPs present a promising drug delivery system for CBD in functional foods, oral medications, and other applications. Moreover, this study reports the remarkable antitumor effects of CBD-SA-BSPs nanomicelles on HCC cells for the first time, laying the foundation for potential applications of CBD in HCC treatment.

Funding: This research was supported by China Postdoctoral Science Foundation (Grant No.2020M673586XB); the Yunnan Major Natural Science Foundation (2019ZF010); the Major Science and Technology Project of Yunnan Province, China (202202AG050009); and Key Laboratory of Chemistry in Ethnic Medicinal Resources (Yunnan Minzu University), State Ethnic Affairs Commission and Ministry of Education (Grant No. 2020MZY05).

Institutional Review Board Statement: Not applicable.

Informed Consent Statement: Not applicable.

Data Availability Statement: Data will be made available on request.

Conflicts of Interest: The authors declare that no conflict of interest exists

Refernces:

[1] F. Bray, J. Ferlay, I. Soerjomataram, R.L. Siegel, L.A. Torre, A. Jemal, Global cancer statistics 2018: GLOBOCAN estimates of incidence and mortality worldwide for 36 cancers in 185 countries, CA Cancer J Clin. 68 (2018) 394-424, https://doi.org/10.3322/caac.21492

[2] Y. Zheng, M. Du, H. Shi, W. Liu, C. Zhuang, H. Chen, Y. Gao, A reactive oxygen/nitrogen species-eliminating natural product-based nanomedicine for prevention and treatment of inflammatory liver injury, Chem. Eng. J. 472 (2023) 144952, https://doi.org/10.1016/j.cej.2023.01.001

[3] J.M. Llovet, J. Zucman-Rossi, E. Pikarsky, B. Sangro, M. Schwartz, M. Sherman, G. Gores, Hepatocellular carcinoma, Nat Rev Dis Primers. 2 (2016) 16018, https://doi.org/10.1038/nrdp.2016.18

[4] A.A. Izzo, F. Borrelli, R. Capasso, V. Di Marzo, R. Mechoulam, Non-psychotropic plant cannabinoids: new therapeutic opportunities from an ancient herb, Trends Pharmacol Sci. 30 (2009) 515-527, https://doi.org/10.1016/j.tips.2009.07.006

[5] P. Massi, M. Solinas, V. Cinquina, D. Parolaro, Cannabidiol as potential anticancer drug, Br J Clin Pharmacol. 75 (2013) 303-312, https://doi.org/10.1111/j.1365-2125.2012.04298.x

[6] R. Ramer, J. Merkord, H. Rohde, B. Hinz, Cannabidiol inhibits cancer cell invasion via upregulation of tissue inhibitor of matrix metalloproteinases-1, Biochem Pharmacol. 79 (2010) 955-966, https://doi.org/10.1016/j.bcp.2009.11.007

[7] E. Kosovic, D. Sykora, M. Kuchar, Stability Study of Cannabidiol in the Form of Solid Powder and Sunflower Oil Solution, Pharmaceutics. 13 (2021) 1-14, https://doi.org/10.3390/pharmaceutics13030412

[8] Y. Nakano, M. Tajima, E. Sugiyama, V.H. Sato, H. Sato, Development of a Novel Nano-emulsion Formulation to Improve Intestinal Absorption of Cannabidiol, Med Cannabis Cannabinoids. 2 (2019) 35-42, https://doi.org/10.1159/000497361

[9] T. Fei, Z. Wan, T. Wang, Dispersing insoluble yolk low-density lipoprotein (LDL) recovered by complexing with carboxymethylcellulose (CMC) for the nanoencapsulation of hemp cannabidiol (CBD) through emulsification at neutral pH, Food Hydrocolloids. 116 (2021) 106656, https://doi.org/10.1016/j.foodhyd.2021.106656

[10] A. Sharkawy, A.M. Silva, F. Rodrigues, F. Barreiro, A. Rodrigues, Pickering emulsions stabilized with chitosan/collagen peptides nanoparticles as green topical delivery vehicles for cannabidiol (CBD), Colloids and Surfaces A: Physicochemical and Engineering Aspects. 631 (2021) 127677, https://doi.org/10.1016/j.colsurfa.2021.127677

[11] P. Lv, D. Zhang, M. Guo, J. Liu, X. Chen, R. Guo, Y. Xu, Q. Zhang, Y. Liu, H. Guo, Structural analysis and cytotoxicity of host-guest inclusion complexes of cannabidiol with three native cyclodextrins, Journal of Drug Delivery Science and Technology. 51 (2019) 337-344, https://doi.org/10.1016/j.jddst.2019.03.015

[12] T.H. Kim, M. Alle, S.C. Park, F. Zhao, W. Long, S. Samala, J.C. Kim, Self-assembly prepared using an ion pair of poly(ethylene imine) and (phenylthio) acetic acid as a drug carrier for oxidation, temperature, and NIR-responsive release, Chem. Eng. J. 415 (2021) 128954. https://doi.org/10.1016/j.cej.2021.128954.

[13] E. Acosta, Bioavailability of nanoparticles in nutrient and nutraceutical delivery, Current opinion in colloid & interface science. 14 (2009) 3-15, https://doi.org/10.1016/j.cocis.2008.01.002

[14] Z. Li, L. Gu, Effects of mass ratio, pH, temperature, and reaction time on fabrication of partially purified pomegranate ellagitannin− gelatin nanoparticles, Journal of agricultural and food chemistry. 59 (2011) 4225-4231, https://doi.org/10.1021/jf200024d

[15] Z. Li, S.S. Percival, S. Bonard, L. Gu, Fabrication of nanoparticles using partially purified pomegranate ellagitannins and gelatin and their apoptotic effects, Molecular nutrition & food research. 55 (2011) 1096-1103, https://doi.org/10.1002/mnfr.201000528

[16] A. Jain, S.K. Singh, S.K. Arya, S.C. Kundu, S. Kapoor, Protein nanoparticles: promising platforms for drug delivery applications, ACS Biomaterials Science & Engineering. 4 (2018) 3939-3961, https://doi.org/10.1021/acsbiomaterials.8b01098

[17] Q. Gu, Y. Liu, L. Zhen, T. Zhao, L. Luo, J. Zhang, T. Deng, M. Wu, G. Cheng, J. Hu, The structures of two glucomannans from Bletilla formosana and their protective effect on inflammation via inhibiting NF-kappaB pathway, Carbohydr Polym. 292 (2022) 119694, https://doi.org/10.1016/j.carbpol.2022.119694

[18] Q. Guan, D. Sun, G. Zhang, C. Sun, M. Wang, D. Ji, W. Yang, Docetaxel-Loaded Self-Assembly Stearic Acid-Modified Bletilla striata Polysaccharide Micelles and Their Anticancer Effect: Preparation, Characterization, Cellular Uptake and In Vitro Evaluation, Molecules. 21 (2016), 1641, https://doi.org/10.3390/molecules21121641

[19] L. Zhao, D. Sun, H. Lu, B. Han, G. Zhang, Q. Guan, In vitro characterization of pH-sensitive Bletilla Striata polysaccharide copolymer micelles and enhanced tumour suppression in vivo, J Pharm Pharmacol. 70 (2018) 797-807, https://doi.org/10.1111/jphp.12888

[20] Q. Guan, G. Zhang, D. Sun, Y. Wang, K. Liu, M. Wang, C. Sun, Z. Zhang, B. Li, J. Lv, In vitro and in vivo evaluation of docetaxel-loaded stearic acid-modified Bletilla striata polysaccharide copolymer micelles, PLoS One. 12 (2017) e0173172, https://doi.org/10.1371/journal.pone.0173172

[21] W. Wang, S. He, T. Hong, Y. Zhang, H. Sui, X. Zhang, Y. Ma, Synthesis, self-assembly, and in vitro toxicity of fatty acids-modified Bletilla striata polysaccharide, Artif Cells Nanomed Biotechnol. 45 (2017) 69-75, https://doi.org/10.3109/21691401.2015.1129621

[22] M. Fernandes Ramos, D. Boston, C.A. Kinney, J.A. Coblinski, F.A. de Oliveira Camargo, Sourcing Cannabis sativa L. by thermogravimetric analysis, Sci Justice. 61 (2021) 401-409, https://doi.org/10.1016/j.scijus.2021.03.002

[23] R. Yang, D. Wang, H. Li, Y. He, X. Zheng, M. Yuan, M. Yuan, Preparation and Characterization of Bletilla striata Polysaccharide/Polylactic Acid Composite, Molecules. 24 (2019), 24(11), https://doi.org/10.3390/molecules24112104

[24] D.M. Andrenyak, D.E. Moody, M.H. Slawson, D.S. O'Leary, M. Haney, Determination of Δ-9-Tetrahydrocannabinol (THC), 11-hydroxy-THC, 11-nor-9-carboxy-THC and Cannabidiol in Human Plasma using Gas Chromatography-Tandem Mass Spectrometry, J Anal Toxicol. 41 (2017) 277-288, https://doi.org/10.1093/jat/bkw136

[25] C.J. Lucas, P. Galettis, J. Schneider, The pharmacokinetics and the pharmacodynamics of cannabinoids, Br J Clin Pharmacol. 84 (2018) 2477-2482, https://doi.org/10.1111/bcp.13710

[26] K.M. Nelson, J. Bisson, G. Singh, J.G. Graham, S.N. Chen, J.B. Friesen, J.L. Dahlin, M. Niemitz, M.A. Walters, G.F. Pauli, The Essential Medicinal Chemistry of Cannabidiol (CBD), J Med Chem. 63 (2020) 12137-12155, https://doi.org/10.1021/acs.jmedchem.0c00724

[27] G. Zhang, J. Qiao, X. Liu, Y. Liu, J. Wu, L. Huang, D. Ji, Q. Guan, Interactions of Self-Assembled Bletilla Striata Polysaccharide Nanoparticles with Bovine Serum Albumin and Biodistribution of Its Docetaxel-Loaded Nanoparticles, Pharmaceutics. 11 (2019), 43, https://doi.org/10.3390/pharmaceutics11010043

[28] C. Wang, C. Dong, Y. Lu, K. Freeman, C. Wang, M. Guo, Digestion behavior, in vitro and in vivo bioavailability of cannabidiol in emulsions stabilized by whey protein-maltodextrin conjugate: Impact of carrier oil, Colloids Surf B Biointerfaces. 223 (2023) 113154, https://doi.org/10.1016/j.colsurfb.2023.113154

[29] F. Schneider, M. Koziolek, W. Weitschies, In Vitro and In Vivo Test Methods for the Evaluation of Gastroretentive Dosage Forms, Pharmaceutics. 11 (2019), https://doi.org/10.3390/pharmaceutics11080416

[30] A.I. Fraguas-Sanchez, A. Fernandez-Carballido, C. Martin-Sabroso, A.I. Torres-Suarez, Stability characteristics of cannabidiol for the design of pharmacological, biochemical and pharmaceutical studies, J Chromatogr B Analyt Technol Biomed Life Sci. 1150 (2020) 122188, https://doi.org/10.1016/j.jchromb.2020.122188

[31] C. Wang, B. Cui, Y. Sun, C. Wang, M. Guo, Preparation, stability, antioxidative property and in vitro release of cannabidiol (CBD) in zein-whey protein composite nanoparticles, LWT. 162 (2022) 113466, https://doi.org/10.1016/j.lwt.2022.113466.

[32] W. Jaidee, I. Siridechakorn, S. Nessopa, V. Wisuitiprot, N. Chaiwangrach, K. Ingkaninan, N. Waranuch, Kinetics of CBD, Delta(9)-THC Degradation and Cannabinol Formation in Cannabis Resin at Various Temperature and pH Conditions, Cannabis Cannabinoid Res. 7 (2022) 537-547, https://doi.org/10.1089/can.2021.0004

[33] L. Grifoni, G. Vanti, R. Donato, C. Sacco, A.R. Bilia, Promising Nanocarriers to Enhance Solubility and Bioavailability of Cannabidiol for a Plethora of Therapeutic Opportunities, Molecules. 27 (2022), 6070, https://doi.org/10.3390/molecules27186070

[34] B. Mukhopadhyay, K. Schuebel, P. Mukhopadhyay, R. Cinar, G. Godlewski, K. Xiong, Cannabinoid receptor 1 promotes hepatocellular carcinoma initiation and progression through multiple mechanisms [J]. Hepatology, 2015, 61(5): 1615-1626, https://doi.org/10.1002/hep.27686

[35] L. García-Morales, A.M. Castillo, J. Tapia Ramírez, H. Zamudio-Meza, M.D.C. Domínguez-Robles, I. Meza, CBD Reverts the Mesenchymal Invasive Phenotype of Breast Cancer Cells Induced by the Inflammatory Cytokine IL-1β [J]. Int J Mol Sci, 2020, 21(7): 2429, https://doi.org/10.3390/ijms21072429

[36] A. Sarkar, A. Mitra, A. Borics, All-Atom Molecular Dynamics Simulations Indicated the Involvement of a Conserved Polar Signaling Channel in the Activation Mechanism of the Type I Cannabinoid Receptor [J]. Int J Mol Sci, 2023, 24(4): 4232, https://doi.org/10.3390/ijms24044232

[37] M. Śmiech, P. Leszczyński, C. Wardell, P. Poznański, M. Pierzchała, H, Taniguchi, Oncogenic Mutation BRAF V600E Changes Phenotypic Behavior of THLE-2 Liver Cells through Alteration of Gene Expression [J]. Int J Mol Sci, 2022, 23(3): 1548, https://doi.org/10.3390/ijms23031548

[38] J. Song, L. Wang, F. Han, The retrospective analysis of rhizoma bletillae used as an antitumor medicine, Inf Tradit Chin Med. 30 (2013) 148-150

[39] J.N. Moreira, R. Gaspar, T.M. Allen, Targeting Stealth liposomes in a murine model of human small cell lung cancer, Biochimica et Biophysica Acta (BBA)-Biomembranes. 1515 (2001) 167-176, https://doi.org/10.1016/S0005-2736(01)00411-4

[40] G.A. Morris, J. Castile, A. Smith, G.G. Adams, S.E. Harding, The effect of prolonged storage at different temperatures on the particle size distribution of tripolyphosphate (TPP)–chitosan nanoparticles, Carbohydrate polymers. 84 (2011) 1430-1434, https://doi.org/10.1016/j.carbpol.2011.01.044

[41] K. Buch, T. Peters, T. Nawroth, M. Sanger, H. Schmidberger, P. Langguth, Determination of cell survival after irradiation via clonogenic assay versus multiple MTT Assay--a comparative study, Radiat Oncol. 7 (2012) 1, https://doi.org/10.1186/1748-717X-7-1

[42] C. Guzman, M. Bagga, A. Kaur, J. Westermarck, D. Abankwa, ColonyArea: an ImageJ plugin to automatically quantify colony formation in clonogenic assays, PLoS One. 9 (2014) e92444, https://doi.org/10.1371/journal.pone.0092444

[43] S. Khazaei, R. Abdul Hamid, N. Mohd Esa, V. Ramachandran, G.T. Aalam, A. Etemad, P. Ismail, Promotion of HepG2 cell apoptosis by flower of Allium atroviolaceum and the mechanism of action, BMC Complement Altern Med. 17 (2017) 104, https://doi.org/10.1186/s12906-017-1594-6